Broadband and Narrow-Band Noise Modeling in Powerline Communications

CHAPTER · DECEMBER 2015

DOI: 10.1002/047134608X.W8289

3 AUTHORS, INCLUDING:

Thokozani Shongwe

University of Johannesburg

15 PUBLICATIONS **37** CITATIONS

SEE PROFILE

A.J: Han Vinck

University of Duisburg-Essen

243 PUBLICATIONS **2,011** CITATIONS

SEE PROFILE

On Broadband and Narrow-band Noise Modelling for OFDM systems in Powerline Communications

Thokozani Shongwe
Department of Electrical and Electronic Engineering Technology, University of Johannesburg, P.O. Box 17011, Doornfontein, 2028, Johannesburg, South Africa
Email: tshongwe@uj.ac.za

A. J. Han Vinck
University of Duisburg-Essen, Institute for Experimental Mathematics, Ellernstr. 29, 45326 Essen, Germany
E-mail: vinck@iem.uni-due.de

Hendrik C. Ferreira
Department of Electrical and Electronic Engineering Science, University of Johannesburg, P.O. Box 524, Auckland Park, 2006, Johannesburg, South Africa
Email: hcferreira@uj.ac.za

***Abstract*—This article gives an overview of noise modelling of the two most problematic types of noise in powerline communications (PLC) namely, impulse noise (broadband noise) and frequency disturbers (narrow-band interference). The models for these two types of noise are studied for OFDM systems. The first part of the article looks at several impulse noise models in the literature. A demonstration of the effects of impulse noise on OFDM, using the Middleton Class A model is given. Methods of combating impulse noise are also studied. In the second part of the article we focus on narrow-band interference (NBI) modelling and also show how NBI affects OFDM systems. The main focus of NBI is on presenting a detailed NBI model because NBI modelling has not been given much attention in the literature. In our discussion of the NBI model we show that, with some assumptions, the NBI model and the Middleton Class A model can be similar.**

***Index Terms*—Impulse noise models, Multi-carrier modulation, Single-carrier modulation, Bernoulli-Gaussian, Middleton Class A, Symmetric alpha-stable distribution, Narrow-band interference, noise model, Powerline communications, OFDM.**

INTRODUCTION

The article is divided into two chapters. The first chapter discusses broadband noise (impulse noise) and its modelling, and the second chapter discusses narrow-band noise and its modelling. In chapter one: this article gives an overview of impulse noise and its models, and points out some important and interesting facts about the study of impulse noise which are sometimes overlooked or not well understood. We discuss the different impulse noise models in the literature, focusing on their similarities and differences when applied in communications systems. The impulse noise models discussed are memoryless (Middleton Class A, Bernoulli-Gaussian and Symmetric alpha-stable), and with memory (Markov-Middleton and Markov-Gaussian). We then go further to give performance comparisons in terms of bit error rates for some of the variants of impulse noise models. We also compare the bit error rate performance of single-carrier (SC) and multi-carrier (MC) communications systems operating under impulse noise. It can be seen that MC is not always better than SC under impulse noise. Lastly, the known impulse noise mitigation schemes (clipping/nulling using thresholds, iterative based and error control coding methods) are discussed. In chapter two: a narrow-band interference (NBI) model for the powerline communications channel is presented. We give frequency domain details and analysis of the NBI model specifically for OFDM systems; it can easily be adapted to model NBI for other communications systems. We also show that by making the same assumptions as in the Middleton class A model, our NBI model becomes the Middleton Class A noise model.

The work in this article is taken from our two papers [1] and [2] which directly resulted in chapters one and two, respectively.

1. BROADBAND NOISE–IMPULSE NOISE

I. INTRODUCTION: IMPULSE NOISE

The effects of impulse noise are experienced by most communications systems. There has been significant research pertaining to impulse noise, which involve modelling of the impulse noise phenomena and combating impulse noise in communications systems. Research articles addressing impulse noise and its effects are found across different fields in communications, some of which are electromagnetic interference, wireless communication, and recently powerline communication. We therefore see it necessary to bring a contribution which gives a general view of impulse noise in communications systems, from the different research fields. The purpose of this chapter is to give an overview of impulse noise, and point out some important and interesting facts about the study of impulse noise which are sometimes overlooked. We begin by looking at the earliest work on impulse noise modelling by Middleton [3, Chapter 11], in Section II. Then we go on to discuss the common impulse noise models in the literature, in Section III, dividing them into those with memory and without memory. We also look at the application of these models with single-carrier and multi-carrier systems. Lastly, we give an overview of the currently known methods of combating impulse noise, in Section IV. This chapter follows from the preliminary work in [4].

II. ON MIDDLETON NOISE MODELLING

The phenomenon of impulse noise was first described in detail by Middleton [3, Chapter 11] in the 1960s, where he

gave a model for impulse noise in communications systems. To obtain the model, Middleton [3, Chapter 11] described impulsive noise in a system as consisting of sequences of pulses (or impulses), of varying duration and intensity, and with the individual pulses occurring more or less random in time. He went further to divide the origin of impulse noise into two categories: (a) Man-made, which is induced by other devices connected in a communications network and (b) naturally occurring, due to atmospheric phenomena and solar static which is due to thunderstorms, sun spots etc. The man-made impulse noise was described as trains of non-overlapping pulses, such as those in pulse time modulation. The impulse noise due to natural phenomena was described as the random superposition of the effects of the individual natural phenomena [3, Chapter 11]. A model for such noise is given in [5], [6] and [7] as

$$n(t) = \sum_{i=1}^{L} a_i \delta(t - t_i), \tag{1}$$

where

- $\delta(t - t_i)$ - is the i_{th} unit (ideal) impulse, described as a delta function.
- a_i - are statistically independent with identical probability density functions (PDFs),
- t_i - are independent random variables uniformly distributed in the time period T_0,
- L - the number of impulses in any observation period T_0, assumed to obey a Poisson distribution

$$P_{T_0}(L) = \frac{(\eta T_0)^L e^{-(\eta T_0)}}{L!}. \tag{2}$$

In (2), η is the average number of impulses per second, and T_0 is the observation period of the impulses. Therefore, ηT_0 is the average number of impulses in the period T_0. It can be seen that the noise model described by (1) is ideal because the impulses are assumed to be delta functions, where $a_i\delta(t - t_i)$ describes the i_{th} impulse of amplitude a_i.

The noise model described by (1) and (2) was originally referred to as the Poisson noise model in [3, Chapter 11], and was widely studied and applied in many systems [5]–[8]. Ziemer [5], utilised the Poisson impulse noise model to calculate error probability characteristics of a matched filter receiver operating in an additive combination of impulsive and Gaussian noise. In [7], the Poisson noise model was used to evaluate the performance of noncoherent M-ary digital systems, ASK, PSK and FSK.

In his later work, Middleton [3] developed statistical noise models which catered for noise due to both man-made and natural phenomena [9]–[11]. In [9] Middleton classified the noise models into the following three categories: *Class A* – the noise has narrower bandwidth than that of the receiver; *Class B* – the noise has larger bandwidth than that of the receiver; *Class C* – the sum of Class A and Class B noise. The most famous of these noise models is the so-called Middleton Class A noise model, which has been widely accepted to model the effects of impulse noise in communications systems. We will, in short, refer to the Middleton Class A model as Class A model.

III. Impulse noise models

Following Middleton's noise models [3, Chapter 11], many authors studied impulse noise modelling. In this section, we discuss some impulse noise models found in the literature. In our discussion of the other impulse noise models we will occasionally mention the Middleton Class A model for reference or comparison purposes as it is a very important model in the study of impulse noise. To date, the following names appear in the literature for different impulse noise models:

1) Impulse noise models without memory
   - Middleton Class A
   - Bernoulli-Gaussian
   - Symmetric Alpha-Stable distribution
2) Impulse noise models with memory
   - Markov-Middleton
   - Markov-Gaussian.

Impulse noise models without memory

A. Middleton Class A

The Class A noise model is still a form of the Poison noise model. However, unlike in (2), the impulse width/duration is taken into account in the Class A noise model as we shall see when studying the impulsive index A. We dedicate space to describing the Class A noise model because it has become the cornerstone of impulse noise modelling and has been extensively studied and utilised in the literature (see [12]–[19].) The Class A noise model gives the probability density function (PDF) of a noise sample, say x_k as follows:

$$F_M(x_k) = \sum_{m=0}^{\infty} P_m \mathcal{N}(x_k; 0, \sigma_m^2), \tag{3}$$

where $\mathcal{N}(x_k; 0, \sigma_m^2)$ represents a Gaussian PDF with mean $\mu = 0$ and variance σ_m^2, from which the k^{th} sample x_k is taken.

$$P_m = \frac{A^m e^{-A}}{m!} \tag{4}$$

and

$$\sigma_m^2 = \sigma_I^2 \frac{m}{A} + \sigma_g^2 = \sigma_g^2 \left(\frac{m}{A\Gamma} + 1 \right), \tag{5}$$

where σ_I^2 is the variance of the impulse noise and σ_g^2 is the variance of the background noise (AWGN). The parameter $\Gamma = \sigma_g^2/\sigma_I^2$ gives the Gaussian to impulse noise power ratio. We can see that the expressions in (2) and (4) are Poisson PDFs. The main difference in (4) is that the term (ηT_0) has been replaced by the parameter A (which does not imply that $A = \eta T_0$). The parameter A here represents the density

of impulses (of a certain width) in an observation period. Therefore

$$A = \frac{\eta\tau}{T_0} = \eta\frac{\tau}{T_0}, \tag{6}$$

where η is the average number of impulses per second (as in (2)), τ is the average duration of each impulse (where all impulses are taken to have the same duration) and τ/T_0 is the fraction of the period T_0 occupied by an impulse of width τ. We now talk of density of impulses instead of number of impulses as done in (2). In (4) we therefore have the densities of impulse noise occurring according to a Poisson distribution.

The density is what has become accepted as "impulsive index", A. The impulsive index is a parameter that is not well explained in the literature. We therefore give some details about the impulsive index, to enhance its understanding. It is worth stating that $A \leq 1$, this follows from the definition of impulsive index being a fraction of impulses in a given observation period T_0. Therefore, for $\eta\tau > T_0$, the impulsive index is capped at 1 no matter how large $\eta\tau$ is, in the observation period T_0.

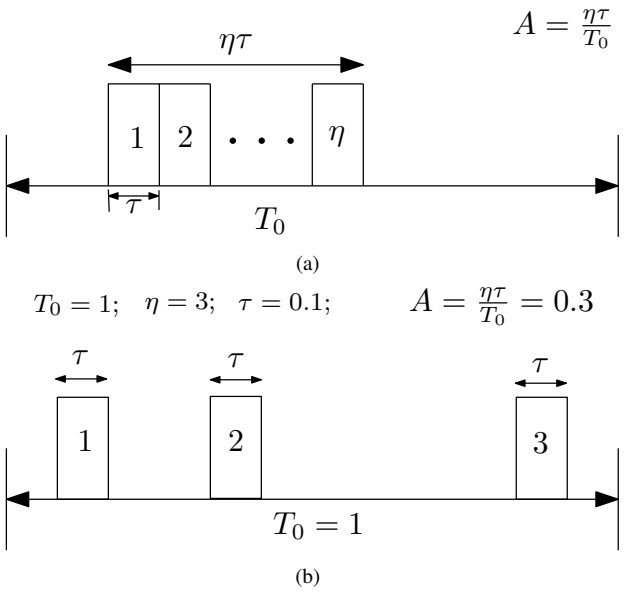

Fig. 1. Example of Impulsive index: (a) Impulsive index (density) of η impulses, each with width (duration) τ, occupying a given time period T_0 and (b) impulsive index (density) of $\eta = 3$ impulses, each with width (duration) $\tau = 0.1$s, occupying a given time period $T_0 = 1$s.

Fig. 1 shows a pictorial view of the impulsive index, A, and what it means. Fig. 1 (a) shows η impulses each of duration τ seconds, where the impulses occur in bursts (next to each other). Fig. 1 (b) shows $\eta = 3$ impulses each of duration $\tau = 0.1$ seconds, where the impulses do not necessarily occur in bursts. We also specify the period of observation as $T_0 = 1$ second in Fig. 1 (b), which is usually the case in the calculation of the impulsive index. The conclusion drawn from Fig. 1 is that whether impulses occur in bursts or not, the calculation of the impulsive index follows the same procedure. In other words, the impulsive index is concerned with the density of impulses in a periodic of observation, not how the impulses are distributed in that period or observation.

B. Bernoulli-Gaussian

The Middleton Class A noise model has already been explained. It can be seen that the PDF of the Class A noise model in (3) is a sum of different zero mean Gaussian PDFs with different variances σ_m^2, where the PDFs are weighted by the Poisson PDF P_m. This summing of weighted Gaussian PDFs is generally referred to as a Gaussian mixture. Another popular impulse noise model, which is a Gaussian mixture according to the Bernoulli distribution, exists in the literature and is called the *Bernoulli-Gaussian* noise model (can be found in [20]–[23].) This noise model is described by the following PDF:

$$F_{BG}(x_k) = (1-p)\mathcal{N}(x_k; 0, \sigma_g^2) + p\mathcal{N}(x_k; 0, \sigma_g^2 + \sigma_I^2). \tag{7}$$

The Bernoulli-Gaussian noise model has similarities to the Class A noise model. To show the similarities, we use the channel models in Fig. 2. Fig. 2 (a) is a two-state representation of the Class A noise model. In the two-state Class A noise model the probability of being in the impulse noise state is A and the average impulse noise variance is σ_I^2. For the two-state Class A noise model, the probability of impulse noise occurrence is found to be A by finding the weighted sum of the probabilities (mP_m) of the Class A noise model: $\sum_{m=1}^{\infty} mP_m = A$. Fig. 2 (b) is a representation the Bernoulli-Gaussian noise model. The models in Fig. 2 look very similar, with the only difference being that in Fig. 2 (b) it is explicitly stated that the noise sample added to the data symbol D_k, in either of the two states, is Gaussian distributed. Whereas in Fig. 2 (a), only the state with variance σ_g^2 can have a Gaussian distribution. However, the state with impulse noise does not necessarily have a Gaussian distribution.

It should be noted that in the impulse noise model in Fig. 2, for the states with impulse noise, the impulse noise variance σ_I^2 is divided by the probability of entering into that state (A or p), such that the impulse noise variance in the system (total number of time samples) becomes σ_I^2. To explain this, let us use the Class A noise model as follows: in the Class A noise model which is defined by (3)–(5), it can be seen that the impulse noise variance of the state m is $(\sigma_I^2 m)/A$ as shown in (5). This variance of state m occurs with probability P_m (see (4)), hence the average impulse noise variance of the Class A noise model is

$$\sum_{m=0}^{\infty} P_m \frac{\sigma_I^2 m}{A} = \frac{\sigma_I^2}{A}\sum_{m=0}^{\infty} mP_m = \frac{\sigma_I^2}{A} \times A = \sigma_I^2. \tag{8}$$

From a simulation point of view, we explain the division of σ_I^2 by A as follows: let us assume a transmission of N symbols. For the impulse noise variance, in the vector of length N, to be approximately σ_I^2, each symbol has to be affected by impulse noise variance σ_I^2/A. It can easily be shown that this situation will result in the impulse noise of σ_I^2 over the

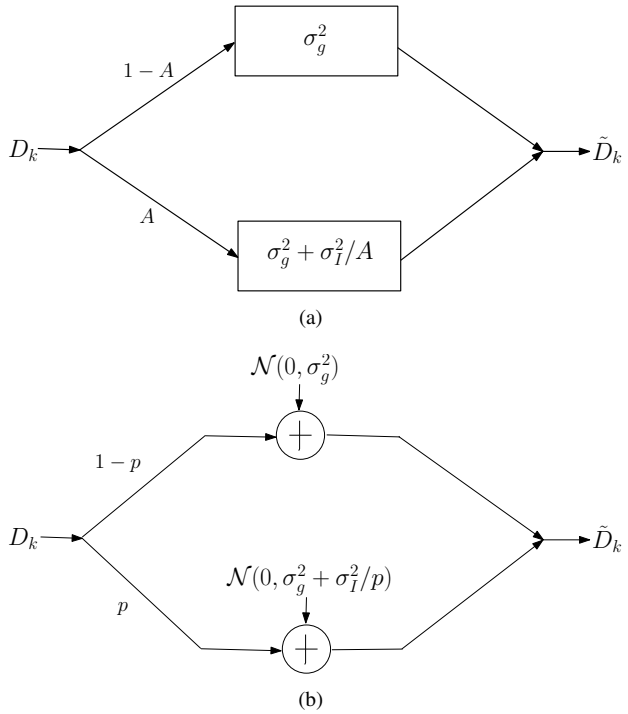

Fig. 2. (a) Two-state Class A noise model and (b) Bernoulli-Gaussian noise model.

N symbols, as follows: we know that impulse noise occurs with probability A, and for N symbols (assuming very large N) we have approximately AN symbols affected by impulse noise of variance σ_I^2/A. This gives the impulse noise variance in N samples as $\sigma_N^2 = AN \times \sigma_I^2/A = N\sigma_I^2$. Then the average impulse noise variance is $\sigma_N^2/N = \sigma_I^2$, which is the result in (8). For the two models in Fig. 2 to be more similar, set $A = p$.

The Bernoulli-Gaussian noise model has been widely adopted in the literature, and some researchers prefer to employ it over the Class A noise model because it is more tractable than the Class A noise model. The Class A model has the advantage of having its parameters directly related to the physical channel. If so desired the Class A model can be adjusted to approximate the Bernoulli-Gaussian, hence giving the Bernoulli-Gaussian model the advantages of the Class A model as well.

The Class A model can also be simplified, and be made more manageable. It was shown in [13] that the PDF of the Class A noise model in (3) can be approximated by the first few terms of the summation and still be sufficiently accurate. Truncating (3) to the first K terms results in the approximation PDF (normalised), which is

$$F_{M,K}(x_k) = \sum_{m=0}^{K-1} P'_m \mathcal{N}(x_k; 0, \sigma_m^2), \tag{9}$$

where

$$P'_m = \frac{P_m}{\sum_{m=0}^{K-1} P_m}.$$

The model in (9) allowed Vastola [13] to design a threshold detector with a simpler structure, which would not have been the case using the model in (3) which has infinite terms. It was also shown in [13] that the first two or three terms are good enough in (9) to approximate the PDF in (3). In [19], the first four terms were used to approximate the PDF of the Class A model. In our simulations, we shall use up to the first five terms of (9), and such a model is shown in Fig. 3.

We now give some results showing the bit error rate (BER) versus SNR when using the model in (9) for different K values. Such results are shown in Figs. 4 and 5, where BPSK modulation is used and $K = 2$, 3 and 5. Figs. 4 and 5 show the effect of different values of A and Γ on the model. In each figure, we use a theoretical BER curve for BPSK as a reference curve against which all curves are compared. The expression for the theoretical BER curve for BPSK is given by (10), where E_b is the signal's bit energy. While our results are limited to BPSK for demonstration purposes, MPSK and MQAM modulations can also be used to obtain BER performances. The general expression for the theoretical BER curve for MPSK is given by (11), where M is the order of the PSK modulation.

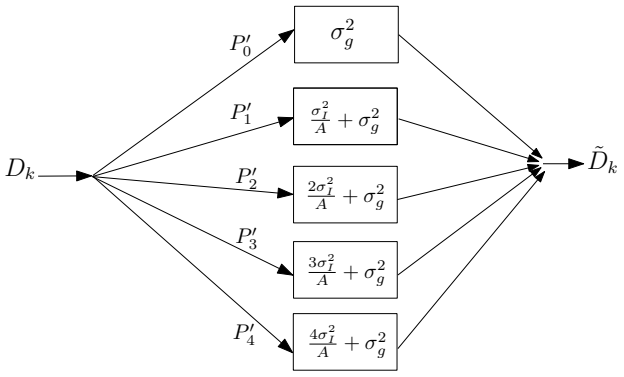

Fig. 3. Five-term, $K = 5$, approximation of the Class A model.

$$\begin{aligned} P_{e,BPSK} &= \frac{(1-A)}{2} Q\left(\sqrt{\frac{E_b}{\sigma_g^2}}\right) \\ &+ \frac{A}{2} Q\left(\sqrt{\frac{E_b}{\sigma_g^2(1+1/AT)}}\right). \end{aligned} \tag{10}$$

$$\begin{aligned} P_{e,MPSK} &\approx \frac{(1-A)}{\mathcal{B}} Q\left(\sqrt{\frac{\mathcal{B}E_b}{\sigma_g^2}} \sin\left(\frac{\pi}{M}\right)\right) \\ &+ \frac{A}{\mathcal{B}} Q\left(\sqrt{\frac{\mathcal{B}E_b}{\sigma_g^2(1+1/AT)}} \sin\left(\frac{\pi}{M}\right)\right), \end{aligned} \tag{11}$$

where $\mathcal{B} = \log_2(M)$.

It can be observed in Figs. 4 and 5 that the model in (9) approximates the Class A model in (3) better for low values of A (see Fig. 4), such that even for two terms, $K = 2$, we get a very good approximation of the theoretical BER curve. For high values of A (see Fig. 5), however, we require more

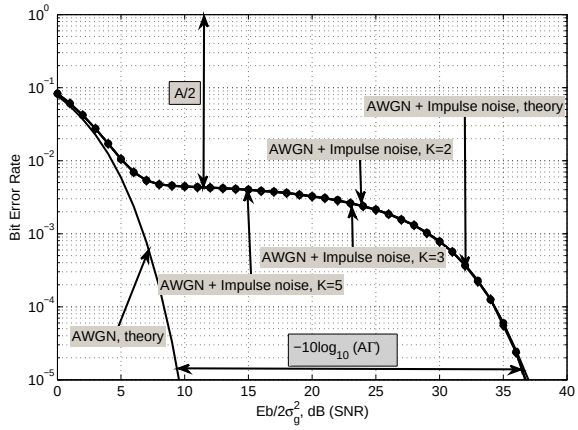

(a) $A = 0.01$, $\Gamma = 0.1$.

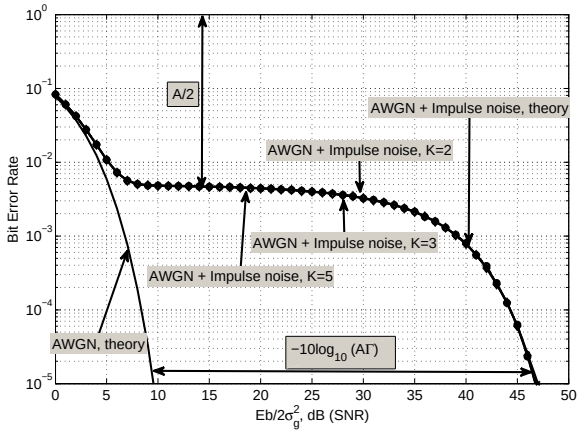

(b) $A = 0.01$, $\Gamma = 0.01$.

Fig. 4. Bit error rate results using the impulse noise model shown in Fig. 3, with $K = 2$, 3 and 5. BPSK was used for the modulation.

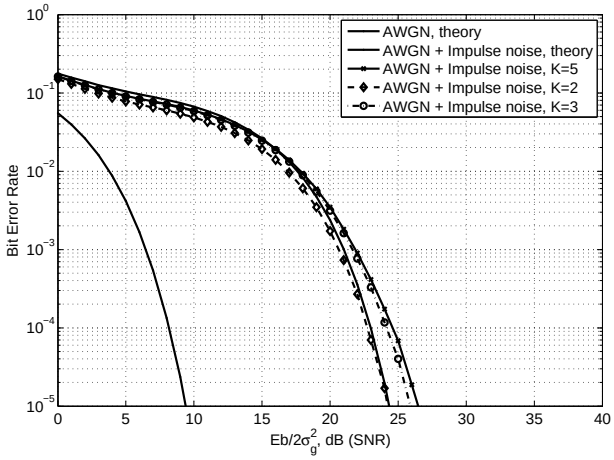

(a) $A = 0.3$, $\Gamma = 0.1$.

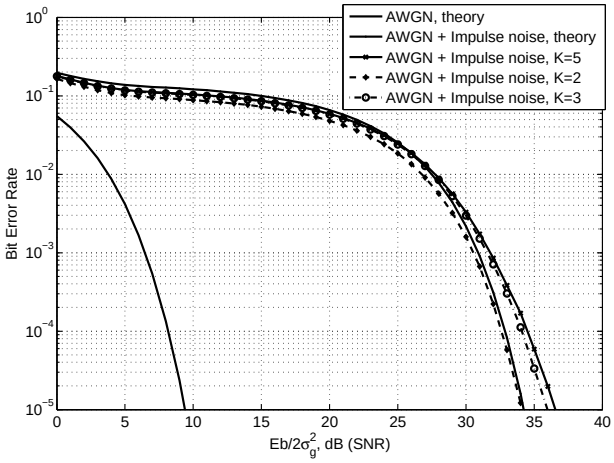

(b) $A = 0.3$, $\Gamma = 0.01$.

Fig. 5. Bit error rate results using the impulse noise model shown in Fig. 3, with $K = 2$, 3 and 5. BPSK was used for the modulation.

terms in (9) to approximate the results of the model in (3), at least for the part of the curve influenced by A (the error floor).

Fig. 5 shows that the results of the $K = 5$ channel model closely approximate the effect of A on the BER curve better than when $K = 2$. This is obviously due to the fact that the more terms (higher K values), the better the approximation of the Class A PDF's probability of impulse noise. However, the $K = 2$ channel model results show a better approximation of the impulse noise power ($1/(A\Gamma)$, which is observed around a BER of 10^{-5}) compared to when $K = 5$. This is because of the m parameter in the term $\sigma_I^2 m/A$ in (5), which influences the impulse noise power. Using more terms in (9) to approximate the results of the model in (3) is more effective in estimating the effect of A in the BERs, but not the impulse noise power.

C. Symmetric alpha(α)-stable distribution for impulse noise modelling

The impulse noise models discussed so far (the Middleton Class A and the Bernoulli-Gaussian) are by far the most widely used in the literature to model impulse noise. There is another impulse noise model that is becoming more common in the literature, and that is the symmetric α-stable (SαS) distribution. This section is therefore a short note on symmetric α-stable distributions used to model impulse noise.

SαS distributions are used in modelling phenomena encountered in practice. These phenomena do not follow the Gaussian distribution, instead their probability distributions may exhibit fat tails when compared to the Gaussian distribution tails [24, Chapter 1]. While stable distributions date back to the 1920s (see [25]), their usage in practical applications had been limited until recently because of their lack of closed-form expressions except for a few (Levy, Cauchy and Gaussian distributions) [24, Chapter 1]. Nowadays powerful computer processors have made it possible to compute stable distributions despite the lack of closed form expressions. This has led to the increasing usage of stable distributions in modelling. Impulse noise is one phenomenon encountered in communication systems which has a probability distribution with fat tails [26]. SαS distributions are therefore considered appropriate for modelling impulse noise [26]–[29].

In this section we give examples of the PDFs of the SαS model for impulse noise, the Class A model and the Bernoulli-Gaussian model. This is meant to show how the SαS model compares, in terms of the PDFs, with the other impulse noise models already discussed.

The SαS distributions are characterised by the following parameters:

- α: is the characteristic exponent, and describes the tail of the distribution ($0 < \alpha \leq 2$).
- β: describes the skewness of the distribution ($-1 \leq \beta \leq 1$); if the distribution is right-skewed ($\beta > 0$) or left-skewed ($\beta < 0$).
- γ: is the scaling parameter ($\gamma > 0$).
- δ: is a real number that gives the location of the distribution. This number tells us where the distribution is located on the x-axis (when the x-axis is used to represent the value of the random variable).

The parameters α and β describe the shape of the distribution; while γ and δ can be thought of as similar to the variance and the mean in a Gaussian distribution, respectively, care should be taken when using these parameters as variance and mean.

When modelling impulse noise using the SαS distribution, the noise is thought of as broadband noise, i.e, the bandwidth of the noise is larger than that of the receiver [30]. Hence, the SαS distribution can be used in the place of the Middleton Class B noise model which requires more (six) parameters to be defined compared to the four parameters required to describe the SαS distribution.

Fig. 6 shows PDFs of the SαS models for different values of α while the other parameters are kept fixed ($\beta = 0$ and $\delta = 0$). The parameter γ is set at $\gamma = 1$ for all PDFs except for the $\alpha = 2$ PDF where $\gamma = 1/\sqrt{2}$. This case of $\alpha = 2$, $\gamma = 1/\sqrt{2}$, $\beta = 0$ and $\delta = 0$ results in the normal distribution as seen in Fig. 6. It should be noted that the SαS distribution of $\alpha = 2$, $\beta = 0$, $\delta = 0$ and $\gamma > 0$ is generally the Gaussian distribution; making the Gaussian distribution a special case of the SαS distributions. Our main aim of presenting Fig. 6 is to show the change of the tails of the SαS PDFs with change in the parameter α and show that the tails are fatter than that of the Gaussian distribution for $\alpha < 2$.

It can be seen in Figs. 6 and 7 that the PDFs of the impulse noise models (Bernoulli-Gaussian, Middleton Class A and SαS) have fat tails. For the Bernoulli-Gaussian and Middleton Class A PDFs, the tails are controlled by the probabilities of impulse noise p and A, respectively; when the probability of impulse noise (p or A) increases, the PDFs tails get fatter. For the SαS PDF, the tails are controlled by the parameter α; with low values of α ($\alpha < 2$) giving PDFs with fatter tails.

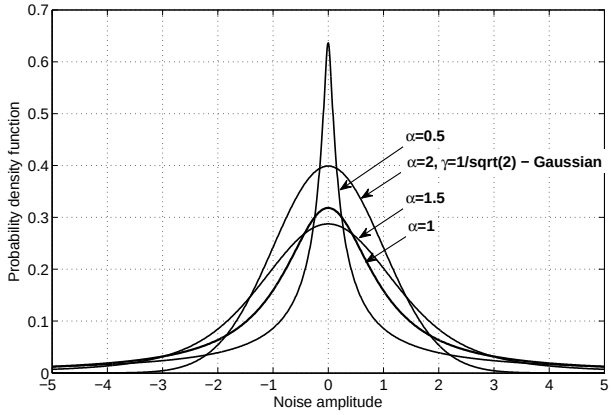

(a) SαS distributions

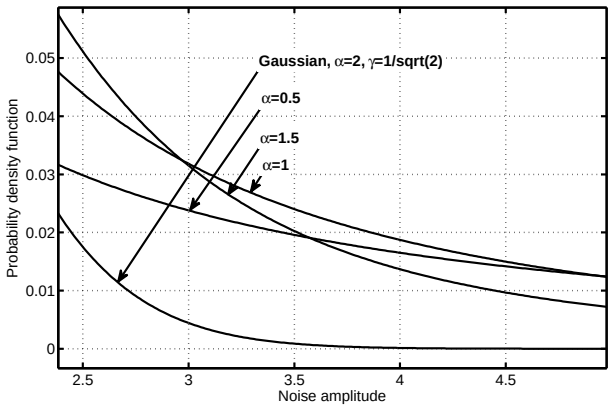

(b) Tails of the distributions

Fig. 6. SαS distributions of different values of α while $\beta = 0$, $\gamma = 1$ and $\delta = 0$. The normal distribution is also included as a SαS distribution of $\alpha = 2$, $\beta = 0$, $\gamma = 1/\sqrt{2}$ and $\delta = 0$.

Impulse noise models with memory

Through measurements in a practical communications channel, Zimmermann and Dostert [31] showed that impulse noise samples sometimes occur in bursts, hence presenting a channel with memory. They further proposed a statistical impulse noise model, based on a partitioned Markov chain, that takes into account the memory nature of impulse noise. Following the work in [31], other authors studied impulse noise with memory as seen in [32], [33], [19] and [34]. In [32], a two-layer two-state Markov model is used to describe bursty impulse noise. The first layer uses a two-state Markov chain to describe the occurrence of impulses and the second layer uses another two-state Markov chain to describe the behaviour of a single impulse. To model impulse noise with memory, Markov chains are invariably used by most authors in the literature. The two models, *Markov-Middleton* [19] and *Markov-Gaussian* [33] are modifications of the Class A and Bernoulli-Gaussian models, respectively, by including Markov chains. Having discussed the impulse noise models without memory, there is no need for a lengthy discussion about the impulse noise models with memory. This is because the impulse noise models with memory are founded on those models without memory. In Fig. 8 we show Markov-Middleton models, which means Class A model with memory. These models in Fig. 8 are an adaptation of the model shown in Fig. 3. The model in Fig. 8 (a) is a "direct" adaptation of the one in Fig. 3, with all the parameters unchanged except for the introduction of memory. However, the model in Fig. 8 (b) [19] allows for all states to be connected such that it is possible to move from one bad state

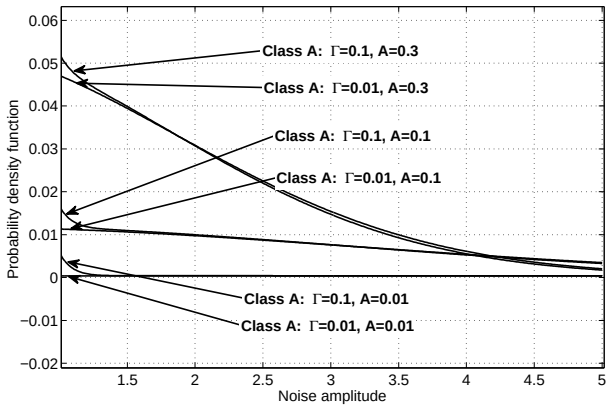

(a) Tails of the PDFs of the Class A model

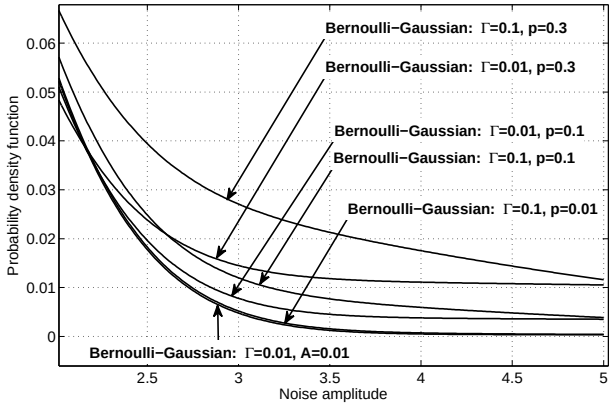

(b) Tails of the PDFs of the Bernoulli-Gaussian model

Fig. 7. Tails of the PDFs of the Class model for different values of A and Γ; tails of the PDFs of the Bernoulli-Gaussian model for different values of p and Γ.

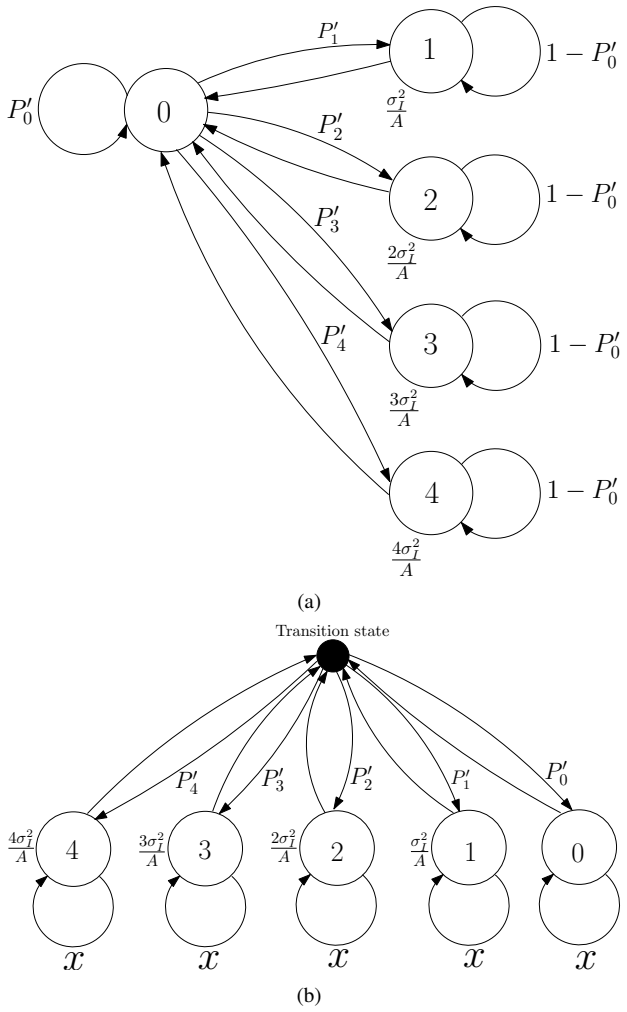

Fig. 8. Markov-Middleton impulse noise models with five terms: (a) is adapted from [35] and (b) is adapted from [19]

(state with impulse noise) to another bad state, which was not possible with the models in Fig. 3 and Fig. 8 (a). With this modification, in Fig. 8 (b), comes a new parameter x, which is independent of the Class A model parameters A, Γ and σ_I^2. The parameter x describes the time correlation between noise samples. The transition state in Fig. 8 (b) has no time duration, it facilitates the connection of the other states. It was shown in [19] that the PDF of their model in Fig. 8 (b) is equivalent to that of Class A model shown in (9).

A Note on Multi-carrier and Single-carrier modulation with Impulse noise

Many authors may correctly argue that the short fall of the Class A and Bernoulli-Gaussian noise models is that they do not take into account the bursty nature of impulse noise. However, for MC modulation it does not matter whether the noise model employed has memory or is memoryless. This is because in MC modulation, the transform (DFT) spreads the time domain impulse noise on all the subcarriers in the frequency domain such that it becomes irrelevant how the noise occurred (in bursts or randomly). This is well explained by Suraweera and Armstrong [36], who showed that the degradation caused by impulse noise in OFDM systems depends only on the total noise energy within one OFDM symbol period, not on the detailed distribution of the noise energy within the symbol. When it comes to SC modulation, however, it may be important to distinguish impulse noise with and without memory.

Here we employ the two-state Class A memoryless model in Fig. 2 (a), with the PDF of the state with impulse noise and AWGN being Gaussian. This makes the model equivalent to the Bernoulli-Gaussian in Fig. 2 (b). In this two-state Class A model, ignoring the effect of the background noise for a moment, we know that the average impulse noise power is $\sigma_I^2 = \sigma_g^2/\Gamma$. The impulse noise power affecting a symbol is $\bar{\sigma}_I^2 = \sigma_I^2/A = \sigma_g^2/A\Gamma$. For discussions and analysis, we will be using the impulse noise power $\bar{\sigma}_I^2 = \sigma_g^2/A\Gamma$.

Given a fixed impulse noise power $\bar{\sigma}_I^2 = \sigma_g^2/A\Gamma$, we vary impulse noise probability A and the impulse noise strength Γ such that $\bar{\sigma}_I^2$ remains the same. This means that if we lower A by a certain amount, we have to increase Γ by the same amount such that the product $A\Gamma$ is unchanged. This we do in order to keep $\bar{\sigma}_I^2$ the same, while observing the effect of changing the

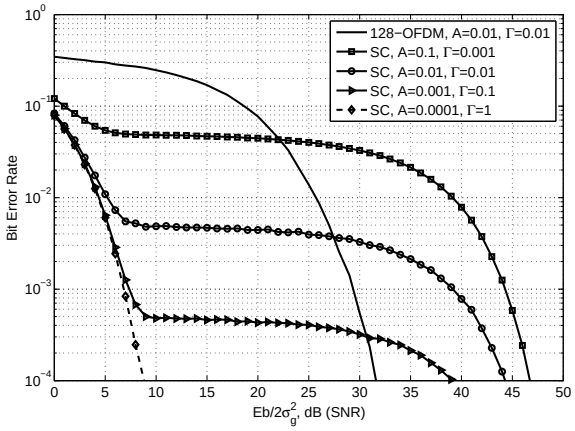

Fig. 9. Comparison of MC and SC modulation in a channel with AWGN and impulse noise of variance $\bar{\sigma}_I^2 = \sigma_g^2/A\Gamma = 1/(0.01 \times 0.01) = 10^4$. $\bar{\sigma}_I^2$ is fixed at 10^4 while different values of A (10^{-1}, 10^{-2}, 10^{-3} and 10^{-4}) are seen to influence the performance of SC modulation.

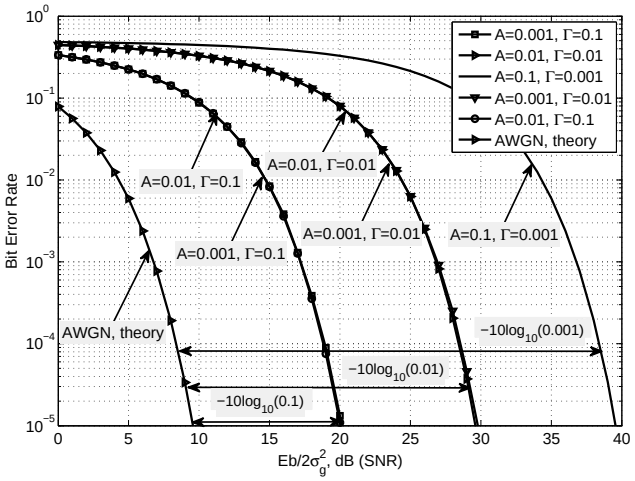

Fig. 10. The results show that with MC modulation the SNR requirement is $\sigma_I^2 = 1/\Gamma$ instead of $1/A\Gamma$, even though a symbol is affected by impulse noise of variance σ_I^2/A . BPSK OFDM was used, with a DFT size of 10000.

probability of impulse noise A on the performance of Single-Carrier and Multi-Carrier Modulation. It is interesting to note that for very low A, SC modulation performs better in the low SNR region compared to MC modulation. However, SC modulation gives an error floor, while MC modulation does not. This behaviour is seen in Fig. 9.

Two important conclusions can be drawn from the behaviour observed in Fig. 9:

- For very low A, very few symbols are affected in SC modulation, hence the low probability of error in SC no matter the strength (or average variance) of the impulse noise. However, with MC modulation, what matters is the average impulse noise variance in the system because the noise power is spread on all subcarriers causing every symbol to be affected by the impulse noise.
- MC modulation has the benefit of eventually outperforming SC modulation as the SNR increases. This is because with MC modulation, the factor $1/A$ does not affect the SNR requirement like in SC modulation. We show this independence from A in MC modulation in Fig. 10.

From the two points above, we can say that MC modulation's performance is independent on the probability of impulse noise occurrence A, while SC modulation's performance shows a strong dependence on A. Therefore, one has to carefully choose between MC and SC modulation depending on the probability of impulse noise that can be tolerated in the communication. By this we mean that if, for example in Fig. 9, $A = 10^{-4}$ and communication is acceptable at probability of error of 10^{-4}, then SC modulation will be the best choice over MC modulation because it will only give an error floor just below A, at $A(M-1)/M$. Ghosh [20] also mentioned that there are conditions where SC modulation performs better than MC modulation. It was also shown in [21], using the Bernoulli-Gaussian noise model, that the impact of impulse noise on the information rate of SC schemes is negligible as long as the occurrence of an impulse noise event is sufficiently small (i.e. very low p in (7).)

IV. Combating Impulse noise

Several techniques for combating impulse noise have been presented in the literature. We shall discuss these techniques in light of MC modulation, OFDM. These techniques fall into the following three broad categories:

1) *Clipping and Nulling (or Blanking)*:
With clipping or nulling, a threshold T_h is used to detect impulse noise in the received signal vector $\mathbf{r}$ before demodulation. Clipping and nulling differ in the action taken when impulse noise is detected in $\mathbf{r}$. If a sample of $\mathbf{r}$, r_k is detected to be corrupted with impulse noise, its magnitude is clipped/limited according to $T_h = T_{\text{clip}}$ (Clipping), or set to zero (Nulling) according to $T_h = T_{\text{null}}$. Given the received sample r_k, then the resulting sample $\tilde{r}_k$, from the clipping technique, is given by

$$\tilde{r}_k = \begin{cases} r_k, & \text{for } |r_k| \leq T_{\text{clip}} \\ T_{\text{clip}} e^{j \arg(r_k)}, & \text{for } |r_k| > T_{\text{clip}} \end{cases},$$

and the resulting sample $\tilde{r}_k$, from the nulling technique, is given by

$$\tilde{r}_k = \begin{cases} r_k, & \text{for } |r_k| \leq T_{\text{null}} \\ 0, & \text{for } |r_k| > T_{\text{null}} \end{cases},$$

where usually $T_{\text{clip}} < T_{\text{null}}$.
Zhidkov [37] gave performance analysis and optimization of blanking (or nulling) for OFDM receivers in the presence of impulse noise, as well as a comparison of clipping, blanking, and combined clipping and blanking in [38]. In [39], the authors advocated for the clipping technique to combat impulse noise in digital television systems using OFDM. The clipping technique, in OFDM, is also seen in [40], where the focus is on deriving and utilising a clipping threshold that does not require the a priori knowledge of the PDF of impulse

noise. Recently, Papilaya and Vinck [41] proposed to include an additional action (with its threshold) to the clipping and nulling actions, which is termed *replacement*. This was done for an OFDM system. The replacement action uses a replacement threshold (T_{rep}) which falls in between the clipping and nulling thresholds, and replaces impulse corrupted samples with the average magnitude of the noiseless OFDM samples.

2) *Iterative*:
With the iterative technique, the idea is to estimate the impulse noise as accurately as possible and then subtract the noise from the received vector $\mathbf{r}$. The noise estimation can be done in the time and/or frequency domains. For good iterative methods, the more iterations the better the estimate of the impulse noise. There is of course a limit to the number of iterations, above which there is little or no improvement in the technique. One of the earliest works on the iterative technique to suppress impulse noise, in OFDM, was by Häring and Vinck [15]. A block diagram of a receiver performing the iterative technique in [15] is shown in Fig. 11 (a). Another application of the iterative technique against impulse noise, in OFDM, is found in [42], where the iterative algorithm is applied in the frequency domain after demodulation and channel equalization.

3) *Error correcting coding*:
Error correcting coding has become a necessary part of any communications system in order to correct errors caused by channel noise. In impulse noise environments, error correcting codes are employed to correct errors caused by impulse noise. Most research on using error correcting codes to combat impulse noise effects in MC systems tend to lean towards convolutional coding [43] [44], Turbo coding [45] [46] and low density parity-check coding [47] [48] or codes that are iteratively decoded [17].

The first two techniques of combating impulse noise, clipping and/or nulling and the iterative technique, are termed *pre-processing* because they process the received vector before the demodulator processing. Error correcting coding (decoding) is not a pre-processing technique, it is implemented after the demodulator to correct errors caused by the impulse noise. It can be used alone or together with the pre-processing techniques.

It has become common practice to implement a combination of the three impulse noise combating techniques above in one system in order to combat impulse noise. Mengi and Vinck [49] employed an impulse noise suppression scheme which combined the iterative technique, and the clipping and nulling techniques, in OFDM. In [50], the iterative and blanking techniques are used together in OFDM. In [40], clipping and error correcting coding are used to combat impulse noise effects in OFDM.

Most impulse noise mitigation schemes have been applied on the memoryless impulse noise models. However, we see very few attempts, in the literature, at combating impulse noise with memory. For an example, in [34] they employed the Markov-Gaussian model for impulse noise and used convolutional error correcting coding.

We give examples of block diagrams of two OFDM systems to illustrate the clipping and/or nulling and iterative techniques in combating impulse noise (see Fig. 11). The figure shows three important points about the clipping and/or nulling and the iterative techniques. Firstly, in Fig. 11 (a) the iterative process is performed to get a good estimate of the noise vector $n^{(l)}$, which is $\tilde{n}^{(l)}$, where l represents the l^{th} iteration. $\tilde{n}^{(l)}$ is found from $n^{(l)}$ using a threshold T as follows: any samples of $n^{(l)}$ that exceed the threshold T are passed on as samples of $\tilde{n}^{(l)}$; any samples of $n^{(l)}$ not exceeding the threshold T are made zero in the corresponding positions in $\tilde{n}^{(l)}$. Using a good estimate of $\tilde{n}^{(l)}$, a more accurate estimate of the desired signal vector $S^{(l)}$ can be obtained. It should be noted that $n^{(l)}$ is found by subtracting the estimated desired signal vector of the l_{th} iteration, $s^{(l)}$ or $S^{(l)}$, from the received vector r or R. Secondly, it should be noted from both Fig. 11 (a) and Fig. 11 (b) that the vector $n^{(l)}$ can be obtained by doing the subtraction of the desired signal vector from the received signal, either in the time or frequency domain. Thirdly, Fig. 11 (b) shows the combination of clipping and/or nulling and iterative technique.

The combination of clipping and/or nulling and iterative technique in Fig. 11 (b) was shown in [49] to give better performance than the iterative technique alone in Fig. 11 (a). In the system in Fig. 11 (b), the clipping and/or nulling is used for the first iteration to significantly improve the estimation of $S^{(l)}$ in the first iteration. This clipping and/or nulling in the first iteration is the reason for the better performance delivered by the system in Fig. 11 (b).

The impulse noise combating techniques discussed have been in light of MC modulation, OFDM. To combat impulse noise in SC modulation, the same techniques can be employed. However, for SC modulation we only see the importance of the impulse noise combating techniques when they are used together with error correcting coding. For example, clipping and/or nulling the impulse noise affected transmitted samples in SC modulation has no effect on the BER performance without coding. This is obviously because the demodulator in SC modulation does not discriminate between high and low amplitude noise when making a decision on the transmitted symbol. The benefit of clipping and/or nulling impulse noise affected samples, in SC modulation is observed when performing soft-decision decoding. Impulse noise in SC modulation has the same effect as narrow-band interference (NBI) in OFDM, considering the NBI model in [51]. Therefore, the same techniques of handling NBI in OFDM found in [51], clipping and/or nulling and error correcting coding, can be used to handle impulse noise in SC modulation. It was shown in [51] that the best technique that gives optimal performance when using a convolutional decoder, is to combine nulling and convolutional soft-decision decoding. Combining clipping and convolutional soft-decision decoding gives suboptimal performance. Impulse noise in SC modulation can be handled exactly the same way. If the impulse noise has memory, the classical

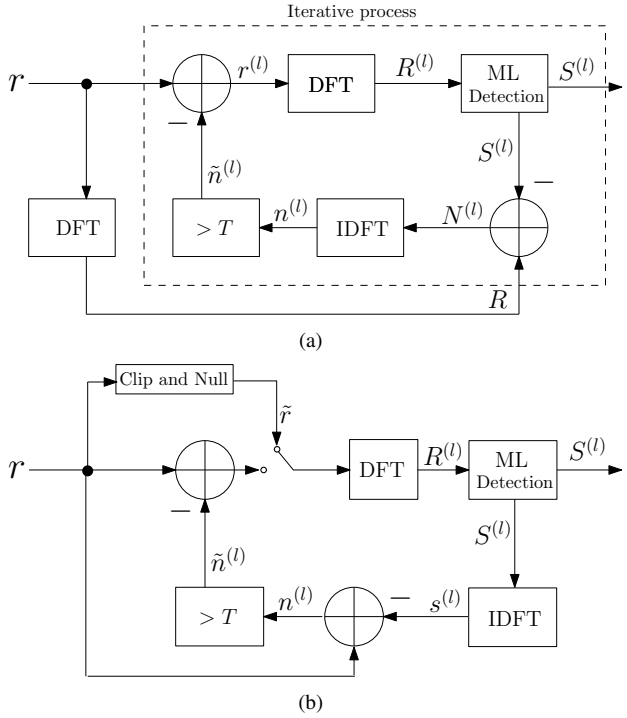

Fig. 11. (a) Iterative impulse noise suppression [15] and (b) Iterative impulse noise suppression with clipping and nulling [49].

interleaver can be employed to randomise the occurrence of errors, hence improving the decoded BER performance.

Focusing on the PLC channel, Vinck [52] proposed the use of a combination of permutation codes and MFSK, to combat impulse noise, as well as other noise types in the PLC channel. This technique was applied in SC modulation, MFSK. Later on, the idea of employing permutation codes with MFSK, in [52], to combat noise typical for a PLC channel (including impulse noise) was taken further in [53] and [54], where powerful permutation codes (called permutation trellis codes) were constructed and used not only to combat impulse noise.

Other impulse noise combating techniques

Another technique used to combat impulse noise in OFDM systems is compressed (or compressive) sensing (CS). With compressed sensing, the idea is to reconstruct a digitized signal using a few of its samples. CS works well with sparse signals. Using CS, the impulse noise in an OFDM signal can be estimated by using pilot subcarriers with their values set to zero. We see the idea of using CS to estimate and cancel impulse noise in OFDM in [55]. In [56] the authors proposed channel estimation working in conjunction with compressed sensing to combat impulse noise for OFDM based power line communication systems. While most research on combating impulse noise focuses on non-bursty impulse noise, Lampe [57] proposed a CS based impulse noise mitigation technique for OFDM that can detect bursty impulse noise. After detecting the impulse noise positions in the OFDM samples, impulse noise cancellation or suppression was applied.

Another technique for combating impulse noise in OFDM, which is similar to compressed sensing, is using the similarity between the DFT (in OFDM) and error correcting codes (particularly Bose-Chaudhuri-Hocquengem and Reed-Solomon codes). This idea, of using the similarities between the DFT and error correcting codes to combat impulse noise, dates back to the 80s where we see Wolf [58] showing that the DFT sequence carries redundant information which can be used to detect and correct errors. Wolf [58] compared the DFT to BCH codes. In [59] the authors show that the OFDM modulator is similar to a Reed-Solomon (RS) encoder and these similarities can be used in OFDM to cancel impulse noise effects. While the scheme in [59] could correct a very limited number of impulse errors because the limitation imposed by the amount of redundancy, an improved scheme with better correcting capabilities was proposed by Mengi and Vinck [60]. The Mengi and Vinck [60] scheme also used OFDM as a RS code, where they proposed to observe not only the subcarriers containing the redundancy symbols but the subcarriers containing information symbols as well.That way their scheme could correct more impulse errors.

V. Conclusion: Impulse noise

Our conclusion is mainly a summary of the interesting facts about impulse noise models. We have also included Table I to summarise some of the important features of the noise models. It should be noted that in Table I the bandwidth of the noise is narrow or broad in reference to the bandwidth of the receiver.

TABLE I
SUMMARY OF THE FEATURES OF THE IMPULSE NOISE MODELS.

	Class A	Bernoulli-Gaussian	SαS
Noise Bandwidth	Narrow-band	not specified	Broad-band
Closed-form expression	exists	exists	does not exists
PDF	exhibits fat tails	exhibits fat tails	exhibits fat tails
Bursty noise modelling	as Markov-Middleton	as Markov-Gaussian	does not model bursty noise

In this chapter we have discussed some important impulse noise models found in the literature. The noise models are divided into those without memory (Middleton Class A and Bernoulli-Gaussian) and those with memory (Markov-Middleton and Markov-Gaussian). We went further to look at the approximation of the PDF of the Middleton Class A model with five terms. We also showed that the Bernoulli-Gaussian model has similarities with the Middleton Class A, and it can be approximated with the Middleton Class A model. We then showed Bit error rate simulation results of the approximation of the Middleton Class A with five terms. Using the Middleton Class A model with five terms we showed equivalent Markov-Middleton models. In addition to the Middleton Class A and Bernoulli-Gaussian models, we also discussed the symmetric alpha(α)-stable distribution

used to model impulse noise. The Symmetric alpha(α)-stable distribution as an impulse noise model was compared with the PDFs of the Middleton Class A and Bernoulli-Gaussian models. All the three models had PDFs that exhibit fat tails. We also showed that single-carrier modulation performs better than multi-carrier modulation under low probability of impulse noise occurrence. With OFDM transmission, it is irrelevant whether the noise occurred in bursts or randomly, what matters is the total noise energy within one OFDM symbol period. Lastly, we discussed impulse noise mitigation schemes: clipping, nulling, iterative and error correcting coding.

2. NARROW-BAND INTERFERENCE

I. INTRODUCTION: NARROW-BAND INTERFERENCE

It is widely accepted that the power line communications channel is characterised by three main noise types namely, coloured background, impulse and narrow-band interference (NBI). Of these three noise types, the narrow-band interference has not been given much attention and as a result it lacks a well defined model. We find some good efforts in describing or modelling narrow-band interference in [61]–[62]. Galda and Rohling [61] gave a brief NBI model description, where the bandwidth of the interfering signal was considered to be small compared to the OFDM subcarrier spacing, hence the interfering signal could be modelled as a single-tone. The frequency and phase of the single-tone interfering signal were assumed to be stochastic with a uniform distribution. The power of the interfering signal was a fixed parameter. In [63], the interfering signal was considered to be a stochastic process in the time domain. The authors in [64] and [65] gave descriptions of interference models together with expressions for the interfering signal. With the aid of the expressions, they explained the conditions under which an interfering signal affects only one subcarrier or several adjacent subcarriers. The work [61]–[65] mostly described the signal processing of the NBI which was sufficient for the purposes of that work. Unfortunately, not much statistical detail of the models was given. The contribution of this chapter is therefore to give a detailed and well-defined narrow-band interference model applicable to an OFDM system, which is an extension of our previous NBI model in [62]. We will focus to the OFDM system when used in the powerline communications (PLC) channel.

Any communications system, with a given finite bandwidth, is susceptible to frequency interference. The frequency interference can originate from several sources and appear on the frequency spectrum of the system as interfering signals. We will call an interfering signal, an *interferer*. In the powerline communications, the sources of frequency interference can be classified into two main classes: 1. interference due to electrical devices connected in the same PLC network as the transmitter of the desired signal, and 2. interference due to radio broadcasters. The devices connected to the PLC network cause interference at their switching frequency and they usually affect PLC transmission taking place in frequencies up hundreds of kilohertz. Radio broadcasters commonly operate in the megahertz region of the frequency spectrum and will interfere with PLC transmission occurring in the megahertz region. In this work, we shall focus on interferers with narrow bandwidth and occurring from independent sources. This view is somewhat generic to the two classes of sources of frequency interference in PLC already mentioned.

Now, we assume that interferers originate from different independent sources, and we also assume that a very large number of interferers rarely occurs within a given frequency band W. We therefore model the probability of a certain number m of interferers on the system's spectrum as a Poisson

distribution

$$P_W(m) = \frac{(\beta W)^m e^{-(\beta W)}}{m!}, \tag{12}$$

where $m = 0, 1, \ldots \infty$. In general, β in (12) is a quantity indicating the average number of occurrences of certain events, defined over a specified observation bandwidth W. The quantities β and W here are equivalent to the one used in (2), which are η and T_0, respectively. In our model, we define the average fraction of bandwidth occupied by NBI in a system bandwidth W as

$$\lambda = \frac{\beta\bar{\Omega}}{W} = \beta\frac{\bar{\Omega}}{W},$$

where β is the average number of interferers, each of average bandwidth $\bar{\Omega}$, and λ is equivalent to the impulsive index A defined in (6). Then we obtain

$$P_m = \frac{\lambda^m e^{-\lambda}}{m!}, \tag{13}$$

where P_m then is the probability that there are m interferers on the frequency band W, which is equivalent to the P_m in (4). The next task is then to find the power of the interferer(s) that affects the system as NBI, and to also approximate the probability distribution of the power of this interference (noise) in the system.

We specify our system of interest in this article as the OFDM (Orthogonal Frequency Division Multiplexing) system, and we shall present our NBI model for this system.

Our NBI model defines the interferers in the frequency domain, with the assumption that they correspond to real signals in the time domain. The effect of the interferers on the system is also completely described in the frequency domain.

OFDM Signal Generation Overview:

OFDM is a multicarrier transmission scheme, where data is carried on several subcarriers which are orthogonal to each other to avoid mutual interference. In the OFDM system of interest, an IDFT (inverse discrete Fourier transform) takes in as input, data symbols D_k, from a phase-shift-keying (PSK) modulation scheme and produces a discrete sequence in the time domain, d_n. The relationship between D_k and d_n is represented by

$$d_n = \frac{1}{\sqrt{N}} \sum_{k=0}^{N-1} D_k e^{j2\pi nk/N}, \tag{14}$$

where N is the number of subcarriers used to carry data. d_n is the complex baseband transmit signal from the output of the IDFT normalized by the factor $\frac{1}{\sqrt{N}}$.

II. NBI Power

Let us define an arbitrary interferer $x(n)$, of bandwidth Ω, as a discrete-time signal which is a sum of arbitrary single-tone signals as

$$x(n) = \sum_{i=0}^{\Omega} A_i e^{j(2\pi f_i n + \phi_i)}, \tag{15}$$

where A_i, f_i and ϕ_i are the corresponding amplitudes, frequencies and phases of the different arbitrary signals, respectively. At the receiver the interferer goes through the N-point DFT and appears on the OFDM spectrum. The result of this operation is described by

$$X(\omega) = \sum_{n=0}^{N-1} x(n) e^{-j\omega n}, \tag{16}$$

where $\omega = r\frac{2\pi}{N}$, for $r = 0 \ldots N-1$. $X(\omega)$ is the amplitude spectrum of $x(n)$ after the DFT. We can represent the continuous amplitude spectrum of $X(\omega)$, in frequency f, as $X(f)$.

If the interferer is a single-tone then it can be described by the i^{th} component in (15) as

$$x_i(n) = A_i e^{j(2\pi f_i n + \phi_i)} \tag{17}$$

and its amplitude spectrum is given by

$$X_i(f) = A_i e^{j\phi_i} e^{j(N-1)(\pi f_i - \pi f)} \frac{\sin N(\pi f_i - \pi f)}{\sin(\pi f_i - \pi f)} \quad [1]. \tag{18}$$

From here onwards, we will refer to the power or amplitude spectrum of a time domain signal (or interferer) after windowing and DFT, simply as power or amplitude spectrum of the signal (interferer).

Now, returning to the amplitude spectrum in (16) which has a bandwidth Ω. We are interested in the effect of the power spectral density (PSD) of the interferer $x(n)$ on the OFDM spectrum and hence, how the interferer affects the OFDM signal as noise in the frequency domain.

In Fig. 12 we show an arbitrary power spectrum of the interferer $x(n)$ denoted by $|X(f)|^2$; together with that of two consecutive subcarriers S_c and S_{c+1}, centred at f_c and f_{c+1}, respectively.

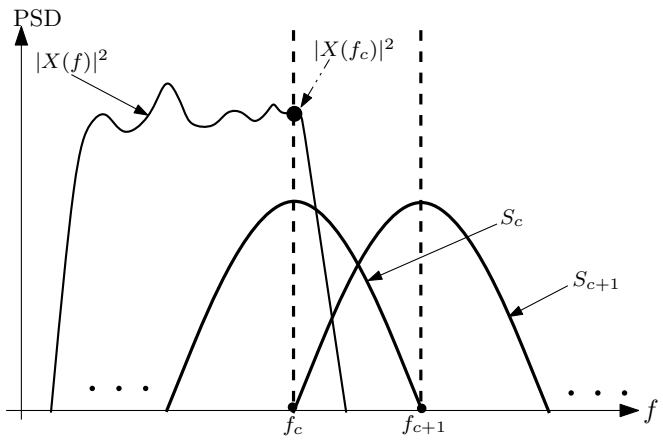

Fig. 12. The effect of the power spectrum $|X(f)|^2$ of an arbitrary interferer $x(n)$, on the OFDM spectrum showing two neighbouring subcarriers S_c and S_{c+1}. The Centre frequencies of S_c and S_{c+1} are f_c and f_{c+1}, respectively. $|X(f_c)|^2$ is the power contribution of the spectrum $|X(f)|^2$, of the interferer, on S_c.

[1]The derivation of the equation can be found in the Appendix

In Fig. 12 we also show some *power contribution* of the interferer on subcarrier S_c as $|X(f_c)|^2$. This power contribution on a subcarrier(s) is the interferer's power that affects the subcarrier as noise or effective noise power. The power contribution $|X(f_c)|^2$ of the interferer on a subcarrier(s) can vary depending on the position of the interferer's PSD on the OFDM spectrum. We will shortly explain this power contribution in relation to the position of a given interferer on a subcarrier.

Focusing on one subcarrier S_c, we are interested in finding the power contribution of the interferer $x(n)$ on the subcarrier, in the frequency domain. The interferer contributes its power to the subcarrier centred at f_c when its power spectrum is evaluated at f_c. This evaluation of the interferer's PSD at f_c results in the power contributed being $|X(f_c)|^2$, as already stated.

It is sufficient to show the power contribution of the interferer(s) on one subcarrier, because the analysis of the power contribution on every other subcarrier follows in the same manner. As such, the analysis of the power contribution on one subcarrier can be applied to all subcarriers.

It should be noted that when the bandwidth of the interferer, Ω is larger than the subcarrier spacing, the interferer may contribute power to several adjacent subcarriers. The contribution of the interferer's power to one subcarrier can be analysed without affecting the contribution to another subcarrier. This is in agreement with our argument that analysing the interferer's power contribution on one subcarrier is enough to give us an understanding of the frequency interference on every subcarrier.

Now, let us have an interferer of fixed average amplitude and bandwidth Ω ($0 < \Omega < W$). This interferer can be located anywhere along the OFDM frequency spectrum W, its position is therefore unknown (variable y). We are interested in finding the noise power contribution of this interferer on a particular subcarrier with a centre frequency f_c. The power contributions of the interferer at f_c are the instantaneous points on the interferer's PSD when evaluated at f_c. Let the position of the interferer, around the subcarrier, have a uniform probability distribution. Since the interferer has bandwidth Ω, then the probability distribution of its power contributions on the subcarrier at f_c, is $P = 2\Omega/W$. Therefore P is a discrete uniform probability distribution. The factor of 2 is due to the fact that the interferer's PSD can be on either side of f_c, in position, and still contribute power at f_c. So, each power contribution of the interferer on a subcarrier has equal probability P, where each power contribution corresponds to the instantaneous location/position of the interferer. This enables us to calculate the average power contribution of the interferer in question on a subcarrier, which will be the sum of all the possible power contributions weighted by the their probabilities P. We denote this average power contribution of a single interferer on subcarrier centred at f_c by $\bar{\chi}$, and it is defined as

$$\begin{aligned} \bar{\chi} &= \int_0^{\Omega} P|X_y(f_c)|^2 dy \\ &= \frac{2\Omega}{W}\int_0^{\Omega} |X_y(f_c)|^2 dy, \end{aligned} \tag{19}$$

where y are the different frequency values (positions on the spectrum) the interferer can assume, which is a variable over the bandwidth of the interferer; $|X_y(f_c)|$ is the amplitude spectrum of the interferer at position y evaluated at the subcarrier centre frequency f_c. The term $\int_0^{\Omega} |X_y(f_c)|^2 dy$ in (19) gives the total power of the interferer, and $\bar{\chi}$ gives the average effective power, which is the power contributed by the interferer on the subcarrier.

To make the analysis simpler for any given number of interferers m, we assume they have an average bandwidth $\Omega = \bar{\Omega}$ and the same amplitude, and hence the same average effective power $\bar{\chi}$ as calculated in (19). Therefore the power contribution, due to the m interferers, is the sum of the average effective power of the individual interferers,

$$\sigma_m^2 = m\bar{\chi}. \tag{20}$$

We call σ_m^2 the effective narrow-band interference (NBI) power, given m interferers. The total average effective NBI power in the system is

$$\begin{aligned} \sigma^2 &= \sum_{m=1}^{\infty} \sigma_m^2 P_m \\ &= \bar{\chi}\sum_{m=1}^{\infty} m P_m \\ &= \bar{\chi}\lambda, \end{aligned} \tag{21}$$

where P_m is as defined in (13) and $\bar{\chi}$ as defined in (19).

Note: If the positions of the interferers are mostly static on the frequency band of interest, as might be the case with the PLC channel, the model will still apply, but with the following changes on the average effective power $\bar{\chi}$ in (19). The position of an interferer will no longer be described by a probability distribution because the interferer's position is fixed (static), and its power that affects a subcarrier centred at f_c will be one of the $|X_y(f_c)|^2$, for $y = 0 \ldots \Omega$. We can define the average effective power, $\bar{\chi}$, as the average of all the values $|X_y(f_c)|^2$, for $y = 0 \ldots \Omega$.

$$\bar{\chi} = E\left\{|X_y(f_c)|^2\right\}, \tag{22}$$

where $E\{.\}$ means the expectation. It should be noted that whether the positions of the interferers are static or changing, that has no bearing on the probability of having interferers in the system, P_m.

A second issue to be noted is that when the average bandwidth of the interferers $\bar{\Omega}$ gets larger, there is likely going to be more adjacent subcarriers affected by an interferer as NBI. Remembering from Section I that $\lambda \propto \bar{\Omega}$, then as $\bar{\Omega}$ gets larger so does λ. This means that the probability of having

NBI in the system increases in proportion to an increased $\bar{\Omega}$. As stated, interferers with larger bandwidth may affect adjacent subcarriers and this will likely result in a burst of errors. Whether adjacent or random subcarriers are affected, the average number of errors that will occur in the system does not change. This burst error phenomenon can easily be taken into account by using models that consider channels with memory for example, a Gilbert-Elliot model.

Similarities to Middleton's Class A Noise Model:

Just as in the Class A noise model discussed in Section III-A, the NBI model in the frequency domain can be seen as an infinite number of parallel channels each with effective NBI power σ_m^2 ($m = 0 \ldots \infty$) and additive white Gaussian noise of variance σ_g^2, where each channel is selected with probability P_m prior to transmission. This channel model is shown in Fig. 13, where a symbol D_k is affected by AWGN of variance σ_g^2 and NBI of variance σ_m^2.

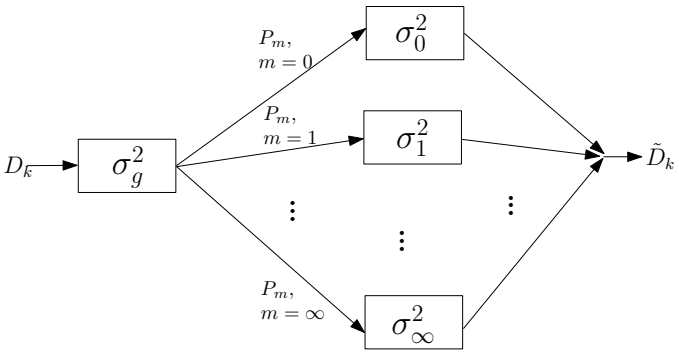

Fig. 13. Narrow-band interference model including additive white Gaussian noise (AWGN). A symbol D_k affected by AWGN of variance σ_g^2. Then it enters one of infinite parallel channels with probability P_m, and in that channel the symbol is affected by NBI of power σ_m^2 such that the output data symbol $\tilde{D}_k$ is the original D_k plus noise of variance $\sigma_g^2 + \sigma_m^2$.

Now, let us make the assumption that the NBI amplitude due to m interferers is a Gaussian random variable, and can take any value n_k, with mean μ and variance σ_m^2. Then this interference (noise) due to m interferers has a Gaussian distribution with a PDF (probability density function) defined as $\mathcal{P}(n_k|m) = \mathcal{N}(n_k; \mu, \sigma_m^2)$.

$$\mathcal{P}(n_k|m) = \frac{1}{\sqrt{2\pi\sigma_m^2}} \exp \frac{-(n_k - \mu)^2}{2\sigma_m^2}. \tag{23}$$

Then the probability distribution of the NBI sample n_k is

$$\begin{aligned} \mathcal{P}(n_k) &= \sum_{m=1}^{\infty} \mathcal{P}(n_k|m) P_m \\ &= \sum_{m=1}^{\infty} P_m \mathcal{N}(n_k; \mu, \sigma_m^2) \end{aligned} \tag{24}$$

With the results of Equation (23) and Equation (24), we have arrived at the same result of Middleton Class A noise model as shown in (3), where it was assumed that the noise has a Gaussian distribution.

III. How the NBI Model is Applied

To demonstrate the application of our NBI model, we shall use an example. Firstly, we modify the infinite-parallel-channel model in Fig. 13 into an easy to use two-parallel-channel (two-state) model as shown in Fig. 14. The model shown in Fig. 14 is similar to the models shown in Fig. 2.

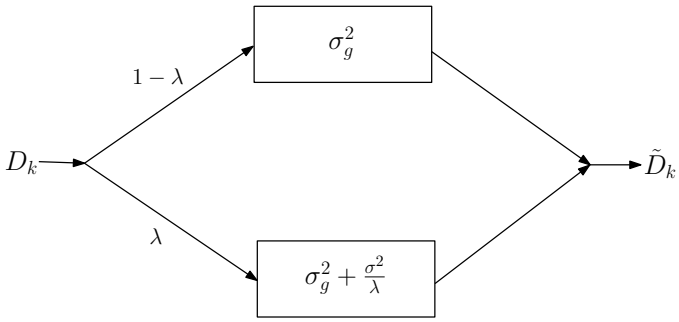

Fig. 14. Narrow-band interference model including additive white Gaussian noise (AWGN). A symbol D_k either enters a channel with AWGN (variance σ_g^2), with probability $1 - \lambda$, or enters a channel with noise $\sigma_g^2 + \sigma^2/\lambda$, with probability λ. σ^2 is the total average effective NBI power in the system as defined in (21).

A transmitted symbol from any modulation is affected by AWGN of variance σ_g^2, with probability $1 - \lambda$. The symbol is affected by AWGN and NBI of average power $\sigma_g^2 + \sigma^2/\lambda$, with probability λ. That is, a symbol "chooses" one of the channels in Fig. 14 according to the entrance probabilities λ or $1 - \lambda$. σ^2 is the total average effective NBI power in the system as defined in (21).

Now, let $\lambda = 10^{-2}$ and $\sigma^2/\lambda = \bar{\chi} = 10$. For AWGN, $\sigma_g^2 = 1$. Having specified the variances of the AWGN and the NBI, we now want to specify the noise samples of the AWGN and that of the NBI, which we call n_g and n_N, respectively. We focus on n_N because n_g is known, it is AWGN.

Let us consider two distributions for the NBI sample n_N, which are the *uniform distribution* and *Gaussian distribution*. This means that the noise sample n_N can be taken from either a uniform or a Gaussian distribution.

Case A: NBI has a uniform distribution.
For a uniform distribution with limits a and b:

- $n_N = a + (b - a)R_u$.
- R_u, a function that generates a random number from a standard uniform distribution on the open interval $(0, 1)$.
- the variance $\sigma^2/\lambda = \bar{\chi}$ is given by $(b - a)^2/12$.
- since we know the variance we need to specify a and b, let $a = -b$, then we have $b = \sqrt{\bar{\chi}}\sqrt{3} = \sqrt{10}\sqrt{3}$.
- $n_N = -\sqrt{10}\sqrt{3} + 2\sqrt{10}\sqrt{3}R_u$.

Case B: NBI has a Gaussian distribution with mean $\mu = 0$.

- $n_N = \sqrt{\mu} + \sqrt{\bar{\chi}}R_g$.
- R_g, a function that generates a random number from a standard normal distribution.
- $n_N = \sqrt{10}R_g$.

The symbol is affected by noise as follows:

- with probability λ: $\tilde{D_k} = n_g + n_N + D_k$
- with probability $1-\lambda$: $\tilde{D_k} = n_g + D_k$,

where $n_g = R_g$ because $\sigma_g^2 = 1$.

If D_k is complex valued, then n_N and n_g have to be complex too. For example, in [62] we generated each NBI sample n_N as a complex random value using the function R_g, such that the sample was $\sqrt{\frac{\sigma^2}{\lambda}}R_g^r + j\sqrt{\frac{\sigma^2}{\lambda}}R_g^c$, where R_g^r and R_g^c indicate that the value generated by R_g is different for the real and complex components of the sample n_N. This means that even though R_g^r and R_g^c are each generated from a standard normal distribution, they are independent. As such, the NBI generated in [62] can be viewed as a random phasor that can rotate in any direction, with the real and imaginary components each having a magnitude determined by R_g and $\sqrt{\frac{\sigma^2}{\lambda}}$.

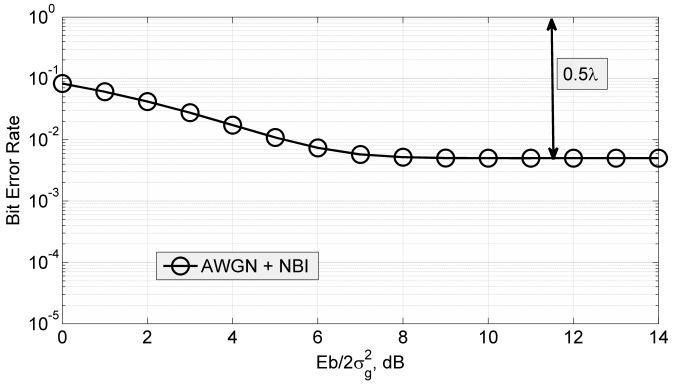

Fig. 15. BPSK–256OFDM modulation bit error rate performance in the presence of NBI with $\sigma^2/\lambda = 10$ and $\lambda = 10^{-2}$, and AWGN with $\sigma_g^2 = 1$.

In Figs. 15 and 16 we give the simulation results of **Case B**, where the system is OFDM with $N = 256$ subcarriers, and BPSK is used as the modulation. In Figs. 15, we set $\lambda = 10^{-2}$ and $\sigma^2/\lambda = 10$. The probability of error caused by NBI for a BPSK modulation will be $0.5 \times \lambda = 0.5 \times 10^{-2}$. The error floor in Fig. 15 confirms this estimate of the probability of error. The Signal to Noise Ratio (SNR) is $Eb/2\sigma_g^2$ in Fig. 15, which does not take into account the NBI power, hence the persistent error floor. The role of Fig. 15 is to indicate the probability of error caused by NBI, which is achieved by not including the NBI power in the SNR. We address the issue of the effect of the NBI power in the SNR in Fig. 16.

Fig. 16 shows the simulation result with similar parameters to that of Fig. 15, except that now the SNR includes the NBI power and is $Eb/2(\sigma_g^2 + \sigma^2/\lambda)$. Also in Fig. 16, we have set $\lambda = 10^{-2}$ and $\sigma^2/\lambda = 100$. The SNR gap between the graph of AWGN only and that of AWGN + NBI confirms the NBI power, $\sigma^2/\lambda = 100$.

IV. Conclusion: Narrow-band interference

We have given a narrow-band interference model which is applicable to the PLC channel when an OFDM system is used. In the model we gave the probability with which this

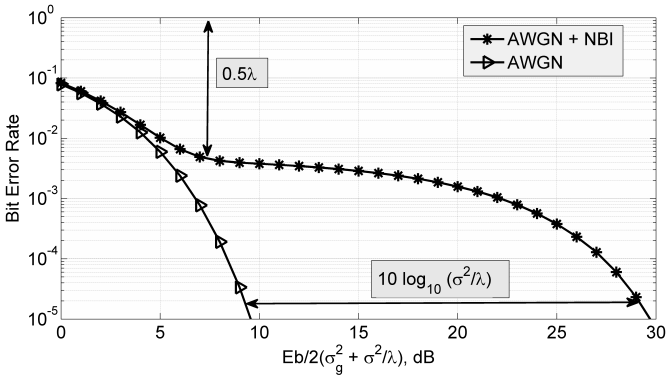

Fig. 16. BPSK–256OFDM modulation bit error rate performance in the presence of NBI with $\sigma^2/\lambda = 100$ and $\lambda = 10^{-2}$, and AWGN with $\sigma_g^2 = 1$.

NBI power affects data. We also showed how to calculate the average effective power of the narrow-band interference, from a number of interferers, that affects the OFDM system. The average effective NBI power can be modelled with an appropriate distribution; in this paper we demonstrated the use of two distributions which were the uniform and Gaussian distribution, and gave numerical results for the Gaussian distribution case.

Conclusion

The article has presented a comprehensive study of noise models for impulse noise and narrow-band interference in OFDM systems. As can be seen, impulse/impulsive noise received more attention from researchers than narrowband interference. This is because researchers view impulse noise as more destructive than narrow-band interference in OFDM systems. It has been shown that with some assumptions, the NBI model (which is in the frequency domain) can be similar to the Middleton Class A noise model (which is in the time domain).

Appendix

Let $x_i(n)$ denote a discrete time signal,

$$x_i(n) = A_i e^{j(\omega_i n + \phi_i)}, \tag{25}$$

where $\omega_i = 2\pi f_i$, A_i is the amplitude and ϕ_i phase of the signal. To simplify the expression we set $A_i = 1$ since it is a constant that does not play any role in the finding of the Fourier transform of $x_i(n)$.

The Fourier transform of $x_i(n)$, $X_i(\omega)$ from an N-point DFT, is

$$
\begin{aligned}
X_i(\omega) &= \sum_{n=0}^{N-1} e^{j(\omega_i n+\phi_i)} e^{-j\omega n} \\
&= e^{j\phi_i} \sum_{n=0}^{N-1} e^{jn(\omega_i-\omega)} \\
&= e^{j\phi_i} \frac{1-e^{jN(\omega_i-\omega)}}{1-e^{j(\omega_i-\omega)}} \\
&= e^{j((\frac{N-1}{2})\omega_i+\phi_i)} e^{-j(\frac{N-1}{2})\omega} \frac{\sin\frac{N}{2}(\omega_i-\omega)}{\sin\frac{1}{2}(\omega_i-\omega)} \\
&= e^{j\phi_i} e^{j\frac{N-1}{2}(\omega_i-\omega)} \frac{\sin\frac{N}{2}(\omega_i-\omega)}{\sin\frac{1}{2}(\omega_i-\omega)},
\end{aligned}
$$

where $\omega = r\frac{2\pi}{N}$, for $r = 0 \ldots N-1$.

REFERENCES

[1] T. Shongwe, A. J. H. Vinck, and H. C. Ferreira, "A study on impulse noise and its models," *SAIEE Africa Research Journal*, 2015, accepted.

[2] T. Shongwe, V. N. Papilaya, and A. J. H. Vinck, "Narrow-band interference model for OFDM systems for powerline communications," in *Proceedings of the 2013 IEEE International Symposium on Power Line Communications and its Applications*, Johannesburg, South Africa, Mar. 24–27, 2013, pp. 268–272.

[3] D. Middleton, *An introduction to statistical communication theory*. McGraw-Hill New York, 1960, vol. 960.

[4] T. Shongwe, A. J. H. Vinck, and H. C. Ferreira, "On impulse noise and its models," in *Proceedings of the 2014 IEEE International Symposium on Power Line Communications*, 2014, pp. 12–17.

[5] R. Ziemer, "Error probabilities due to additive combinations of Gaussian and impulsive noise," *IEEE Transactions on Communication Technology*, vol. 15, no. 3, pp. 471–474, June 1967.

[6] ——, "Character error probabilities for M-ary signaling in impulsive noise environments," *IEEE Transactions on Communication Technology*, vol. 15, no. 1, pp. 32–34, Feb. 1967.

[7] H. Huynh and M. Lecours, "Impulsive noise in noncoherent M-ary digital systems," *IEEE Transactions on Communications*, vol. 23, no. 2, pp. 246–252, Feb. 1975.

[8] S. A. Kosmopoulos, P. T. Mathiopoulos, and M. D. Gouta, "Fourier-Bessel error performance analysis and evaluation of M-ary QAM schemes in an impulsive noise environment," *IEEE Transactions on Communications*, vol. 39, no. 3, pp. 398–404, Mar. 1991.

[9] D. Middleton, "Statistical-physical models of electromagnetic interference," *IEEE Transactions on Electromagnetic Compatibility*, vol. 19, no. 3, pp. 106–127, Aug. 1977.

[10] ——, "Procedures for determining the parameters of the first-order canonical models of class A and class B electromagnetic interference," *IEEE Transactions on Electromagnetic Compatibility*, vol. 21, no. 3, pp. 190–208, Aug. 1979.

[11] ——, "Canonical and quasi-canonical probability models of class A interference," *IEEE Transactions on Electromagnetic Compatibility*, vol. 25, no. 2, pp. 76–106, May 1983.

[12] L. A. Berry, "Understanding Middleton's canonical formula for class A noise," *IEEE Transactions on Electromagnetic Compatibility*, vol. 23, no. 4, pp. 337–344, Nov. 1981.

[13] K. Vastola, "Threshold detection in narrow-band non-Gaussian noise," *IEEE Transactions on Communications*, vol. 32, no. 2, pp. 134–139, Feb. 1984.

[14] S. Miyamoto, M. Katayama, and N. Morinaga, "Performance analysis of QAM systems under class A impulsive noise environment," *IEEE Transactions on Electromagnetic Compatibility*, vol. 37, no. 2, pp. 260–267, May 1995.

[15] J. Häring and A. J. H. Vinck, "OFDM transmission corrupted by impulsive noise," in *Proceedings of the 2000 International Symposium on Power-Line Communications and its Applications*, Limerick, Ireland, Apr. 5–7, 2000, pp. 5–7.

[16] ——, "Performance bounds for optimum and suboptimum reception under Class-A impulsive noise," *IEEE Transactions on Communications*, vol. 50, no. 7, pp. 1130–1136, July 2002.

[17] ——, "Iterative decoding of codes over complex numbers for impulsive noise channels," *IEEE Transactions on Information Theory*, vol. 49, no. 5, pp. 1251–1260, May 2003.

[18] K. C. Wiklundh, P. F. Stenumgaard, and H. M. Tullberg, "Channel capacity of Middleton's class A interference channel," *Electronics letters*, vol. 45, no. 24, pp. 1227–1229, Nov. 2009.

[19] G. Ndo, F. Labeau, and M. Kassouf, "A Markov-Middleton model for bursty impulsive noise: Modeling and receiver design," *IEEE Transactions on Power Delivery*, vol. 28, no. 4, pp. 2317–2325, Oct. 2013.

[20] M. Ghosh, "Analysis of the effect of impulse noise on multicarrier and single carrier QAM systems," *IEEE Transactions on Communications*, vol. 44, no. 2, pp. 145–147, Feb. 1996.

[21] R. Pighi, M. Franceschini, G. Ferrari, and R. Raheli, "Fundamental performance limits of communications systems impaired by impulse noise," *IEEE Transactions on Communications*, vol. 57, no. 1, pp. 171–182, Jan. 2009.

[22] T. Y. Al-Naffouri, A. A. Quadeer, and G. Caire, "Impulsive noise estimation and cancellation in DSL using orthogonal clustering," in *Proceedings of the 2011 IEEE International Symposium on Information Theory*, Saint Petersburg, Russia, July 31–Aug. 5, 2011, pp. 2841–2845.

[23] S. P. Herath, N. H. Tran, and T. Le-Ngoc, "On optimal input distribution and capacity limit of Bernoulli-Gaussian impulsive noise channels," in *Proceedings of the 2012 IEEE International Conference on Communications*, Ottawa, ON, Canada, June 10–15, 2012, pp. 3429–3433.

[24] J. P. Nolan, *Stable Distributions: Models for Heavy-Tailed Data*. Boston: Birkhauser, 2007.

[25] P. Levy, *Calcul des Probabilites*. Paris: Gauthier-Villars, 1925.

[26] C. L. Brown and A. M. Zoubir, "A nonparametric approach to signal detection in impulsive interference," *IEEE Transactions on Signal Processing*, vol. 48, no. 9, pp. 2665–2669, 2000.

[27] G. A. Tsihrintzis and C. L. Nikias, "Performance of optimum and suboptimum receivers in the presence of impulsive noise modeled as an alpha-stable process," *IEEE Transactions on Communications*, vol. 43, no. 234, pp. 904–914, 1995.

[28] E. E. Kuruoglu, W. J. Fitzgerald, and P. J. Rayner, "Near optimal detection of signals in impulsive noise modeled with a symmetric α-stable distribution," *IEEE Communications Letters*, vol. 2, no. 10, pp. 282–284, 1998.

[29] J. Ilow and D. Hatzinakos, "Analytic alpha-stable noise modeling in a Poisson field of interferers or scatterers," *IEEE Transactions on Signal Processing*, vol. 46, no. 6, pp. 1601–1611, 1998.

[30] D. Middleton, "Non-Gaussian noise models in signal processing for telecommunications: new methods an results for class A and class B noise models," *IEEE Transactions on Information Theory*, vol. 45, no. 4, pp. 1129–1149, 1999.

[31] M. Zimmermann and K. Dostert, "Analysis and modeling of impulsive noise in broad-band powerline communications," *IEEE Transactions on Electromagnetic Compatibility*, vol. 44, no. 1, pp. 249–258, Feb. 2002.

[32] P. Amirshahi, M. S. Navidpour, and M. Kavehrad, "Performance analysis of uncoded and coded OFDM broadband transmission over low voltage power-line channels with impulsive noise," *IEEE Transactions on Power Delivery*, vol. 21, no. 4, pp. 1927–1934, Oct. 2006.

[33] D. Fertonani and G. Colavolpe, "On reliable communications over channels impaired by bursty impulse noise," *IEEE Transactions on Communications*, vol. 57, no. 7, pp. 2024–2030, July 2009.

[34] J. Mitra and L. Lampe, "Convolutionally coded transmission over Markov-Gaussian channels: Analysis and decoding metrics," *IEEE Transactions on Communications*, vol. 58, no. 7, pp. 1939–1949, July 2010.

[35] H. C. Ferreira, L. Lampe, J. Newbury, and T. G. Swart, *Power Line Communications: Theory and Applications for Narrowband and Broadband Communications Over Power Lines*. Chichester, England: John Wiley and Sons, 2010.

[36] H. A. Suraweera and J. Armstrong, "Noise bucket effect for impulse noise in OFDM," *Electronics Letters*, vol. 40, no. 18, pp. 1156–1157, Sept. 2004.

[37] S. V. Zhidkov, "Performance analysis and optimization of OFDM receiver with blanking nonlinearity in impulsive noise environment," *IEEE Transactions on Vehicular Technology*, vol. 55, no. 1, pp. 234–242, Jan. 2006.

[38] ——, "Analysis and comparison of several simple impulsive noise mitigation schemes for OFDM receivers," *IEEE Transactions on Communications*, vol. 56, no. 1, pp. 5–9, Jan. 2008.

[39] H. A. Suraweera, C. Chai, J. Shentu, and J. Armstrong, "Analysis of impulse noise mitigation techniques for digital television systems," in *Proceedings the 8th international OFDM Workshop*, Hamburg, Germany, Sept. 2003, pp. 172–176.

[40] D.-F. Tseng, Y. S. Han, W. H. Mow, L.-C. Chang, and A. J. H. Vinck, "Robust clipping for OFDM transmissions over memoryless impulsive noise channels," *IEEE Communications Letters*, vol. 16, no. 7, pp. 1110–1113, July 2012.

[41] V. N. Papilaya and A. J. H. Vinck, "Investigation on a new combined impulsive noise mitigation scheme for OFDM transmission," in *Proceedings of the 2013 IEEE International Symposium on Power Line Communications*, Johannesburg, South Africa, Mar. 24–27, 2013, pp. 86–91.

[42] S. V. Zhidkov, "Impulsive noise suppression in OFDM-based communication systems," *IEEE Transactions on Consumer Electronics*, vol. 49, no. 4, pp. 944–948, Nov. 2003.

[43] D. H. Sargrad and J. W. Modestino, "Errors-and-erasures coding to combat impulse noise on digital subscriber loops," *IEEE Transactions on Communications*, vol. 38, no. 8, pp. 1145–1155, Aug. 1990.

[44] T. Li, W. H. Mow, and M. Siu, "Joint erasure marking and viterbi decoding algorithm for unknown impulsive noise channels," *IEEE Transactions on Wireless Communications*, vol. 7, no. 9, pp. 3407–3416, Sept. 2008.

[45] T. Faber, T. Scholand, and P. Jung, "Turbo decoding in impulsive noise environments," *Electronics letters*, vol. 39, no. 14, pp. 1069–1071, July 2003.

[46] A. Burnic, A. Hessamian-Alinejad, T. Scholand, T. E. Faber, G. H. Bruck, and P. Jung, "Error correction in impulsive noise environments by applying turbo codes," in *Proceedings of the 2006 IEEE International Symposium on Personal, Indoor and Mobile Radio Communications*, Helsinki, Finland, Sept. 11–14, 2006, pp. 1–5.

[47] H. Nakagawa, D. Umehara, S. Denno, and Y. Morihiro, "A decoding for low density parity check codes over impulsive noise channels," in *Proceedings of the 2005 International Symposium on Power Line Communications*, Vancouver, Canada, Apr. 6–8, 2005, pp. 85–89.

[48] H.-M. Oh, Y.-J. Park, S. Choi, J.-J. Lee, and K.-C. Whang, "Mitigation of performance degradation by impulsive noise in LDPC coded OFDM system," in *Proceedings of the 2006 IEEE International Symposium on Power Line Communications*, Orlando, Florida, USA, Mar. 26–29, 2006, pp. 331–336.

[49] A. Mengi and A. J. H. Vinck, "Successive impulsive noise suppression in OFDM," in *Proceedings of the 2009 IEEE International Symposium on Power Line Communications*, Rio de Janeiro, Brazil, Mar. 5–7, 2009, pp. 33–37.

[50] C.-H. Yih, "Iterative interference cancellation for OFDM signals with blanking nonlinearity in impulsive noise channels," *IEEE Signal Processing Letters*, vol. 19, no. 3, pp. 147–150, Mar. 2012.

[51] T. Shongwe and A. J. H. Vinck, "Interleaving and nulling to combat narrow-band interference in PLC standard technologies PLC G3 and PRIME," in *Proceedings of the 2013 IEEE International Symposium on Power Line Communications*, Johannesburg, South Africa, Mar. 24–27, 2013, pp. 258–262.

[52] A. J. H. Vinck, "Coded modulation for powerline communications," *AEÜ International Journal of Electronics and Communications*, vol. 54, no. 1, pp. 45–49, Jan. 2000.

[53] H. C. Ferreira and A. J. H. Vinck, "Interference cancellation with permutation trellis codes," in *Proceedings of the 2000 IEEE Vehicular Technology Conference*, Boston, MA, USA, Sept. 24–28, 2000, pp. 2401–2407.

[54] H. C. Ferreira, A. J. H. Vinck, T. G. Swart, and I. de Beer, "Permutation trellis codes," *IEEE Transactions on Communications*, vol. 53, no. 11, pp. 1782–1789, Nov. 2005.

[55] G. Caire, T. Y. Al-Naffouri, and A. K. Narayanan, "Impulse noise cancellation in ofdm: an application of compressed sensing," in *Proceedings of the 2008 IEEE International Symposium on Information Theory*, Toronto, ON, Canada, July 6–11, 2008, pp. 1293–1297.

[56] A. Mehboob, L. Zhang, J. Khangosstar, and K. Suwunnapuk, "Joint channel and impulsive noise estimation for OFDM based power line communication systems using compressed sensing," in *Proceedings of the 2013 IEEE International Symposium on Power Line Communications*, Johannesburg, South Africa, Mar. 24–27, 2013, pp. 203–208.

[57] L. Lampe, "Bursty impulse noise detection by compressed sensing," in *Proceedings of the 2011 IEEE International Symposium on Power Line Communications*, Udine, Italy, Apr. 3–6, 2011, pp. 29–34.

[58] J. Wolf, "Redundancy, the discrete Fourier transform, and impulse noise cancellation," *IEEE Transactions on Communications*, vol. 31, no. 3, pp. 458–461, Mar. 1983.

[59] F. Abdelkefi, P. Duhamel, and F. Alberge, "Impulsive noise cancellation in multicarrier transmission," *IEEE Transactions on Communications*, vol. 53, no. 1, pp. 94–106, Jan. 2005.

[60] A. Mengi and A. J. H. Vinck, "Impulsive noise error correction in 16-OFDM for narrowband power line communication," in *Proceedings of the 2009 IEEE International Symposium on Power Line Communications*, Dresden, Germany, Mar. 29–Apr. 1, 2009, pp. 31–35.

[61] D. Galda and H. Rohling, "Narrow band interference reduction in OFDM-based power line communication systems," in *Proceedings of the 2011 IEEE International Symposium on Power Line Communications*, Malmo, Sweden, Apr. 4–6, 2001, pp. 345–351.

[62] V. N. Papilaya, T. Shongwe, A. J. H. Vinck, and H. C. Ferreira, "Selected subcarriers QPSK-OFDM transmission schemes to combat frequency disturbances," in *Proceedings of the 2012 IEEE International Symposium on Power Line Communications and its Applications*, Beijing, China, Mar. 27–30, 2012, pp. 200–205.

[63] R. Nilsson, F. Sjoberg, and J. P. LeBlanc, "A rank-reduced LMMSE canceller for narrowband interference suppression in OFDM-based systems," *IEEE Transactions on Communications*, vol. 51, no. 12, pp. 2126–2140, Dec. 2003.

[64] A. J. Coulson, "Bit error rate performance of OFDM in narrowband interference with excision filtering," *IEEE Transactions on Wireless Communications*, vol. 5, no. 9, pp. 2484–2492, Sept. 2006.

[65] C. Snow, L. Lampe, and R. Schober, "Error rate analysis for coded multicarrier systems over quasi-static fading channels," *IEEE Transactions on Communications*, vol. 55, no. 9, pp. 1736–1746, Sept. 2007.